Quantum Electronics **52** (3) 269–273 (2022)

https://doi.org/10.1070/QEL17996

Study of second optical harmonic generation in terahertz pulse-induced antiferromagnetic NiO

O.V. Chefonov, A.V. Ovchinnikov, M.B. Agranat

Abstract. **Intense terahertz pulses and a process of second harmonic generation are promising methods for exciting and studying an ultrafast dynamic response in magnetically ordered systems, ferroelectrics, and multiferroics on the picosecond time scale. In the present work, we report experimental results on generation of second optical harmonic in centrosymmetric antiferromagnetic NiO induced by intense terahertz pulses with an electric field strength of up to 20 MV cm^{-1}.**

Keywords: *second harmonic generation, antiferromagnetic, femtosecond laser pulse, terahertz pulse, pump–probe.*

1. Introduction

Second harmonic generation (SHG) is widely used for studying properties of crystals and thin films [1, 2]. Nonlinear effects and related measurements have a high sensitivity to variations in electric and magnetic symmetry, crystallographic orientation, and polarisation under an external action [3–7]. A high sensitivity of SHG and its selectivity with respect to bulk and interface properties of an object under study may in some cases excess those obtained with other methods [8]. Earlier, Ovchinnikov et al. reported [6] about the observation of second harmonic generation at a wavelength of 620 nm under the action of terahertz (THz) pulsed radiation in centrosymmetric antiferromagnetic NiO at room temperature. In the present work, we submit experimental results on studying second optical harmonic generation in centrosymmetric antiferromagnetic NiO under the action of THz radiation pulses with an electric field strength of up to 20 MV cm^{-1}. The study of SHG in a NiO sample was performed by using the double-pulse pump–probe method. In this method, terahertz pulses were used as the pump pulses, and for probe pulses, counter-propagating femtosecond laser pulses were employed (in contrast to paper [6]) at a radiation wavelength of 1240 nm.

2. Experimental

In experiments, a Cr:forsterite femtosecond laser system was used, which generated pulses at a radiation wavelength of 1240 nm, with a duration of 100 fs, an energy of above 40 mJ, and a pulse repetition rate of 10 Hz [9]. The experimental scheme is shown in Fig. 1. With a wedged beam splitter plate, the laser radiation was divided into two parts after the amplification stages. The main part of the laser pulse energy (98%) was used for generating THz pulses, and the rest of energy (2%) served as a probe radiation for studying SHG. The THz pulsed generation was realised by the optical rectification method applied to femtosecond laser pulses in a composed organic nonlinear crystal DSTMS [10]. The energies of the probe pulse and the pulse pumping the crystal DSTMS (monitoring the THz radiation energy) were controlled by polarisation attenuators comprised of a Glan–Thompson prism and a half-wave plate. After the DSTMS crystal, a cutting broadband THz filter (LPF8.8-47, Tydex) was placed in the path of the THz beam, which blocked radiation at wavelengths shorter than 34 μm with an attenuation factor of above 10^8. For obtaining a maximum electric field strength, the beam of THz radiation was expanded from the initial 8 to 48 mm by a telescope consisting of two off-axis parabolic mirrors with effective focal lengths of 25.4 and 152.4 mm, respectively. The radiation was focused on a sample by an off-axis parabolic mirror with an effective focal length of 50.8 mm and a diameter of 50.8 mm. In the focal plane, the size of the THz beam was 170 ± 10 μm with respect to the 1/e level, which is close to the diffraction limit of 154 μm (for a centre wavelength of 170 μm). A spatial distribution of the THz beam was measured by a specialised camera RIGI (Swiss Terahertz). An energy of the THz pulses in the focal plane, incident onto the sample and passed through it, was controlled by an image transfer system, which included two 50.8-mm-diameter off-axis parabolic mirrors with the effective focal lengths of 50.8 and 76.1 mm, respectively, and a calibrated Golay cell (GC-1D, Tydex).

The waveform of THz pulses was measured by the electro-optical sampling in a gallium phosphide crystal GaP (110) of thickness 100 μm, which was attached to a GaP (100) substrate of thickness 2 mm on an optical contact. The waveform and spectrum of THz pulses are shown in Fig. 2. The maximal electric field strength of THz pulses in the experiments was 19 MV cm^{-1}. The electric field intensity of the pulses was estimated from measured values of energy, duration, and spot size.

The probe optical pulse propagated in the opposite direction with respect to that of a THz pulse. Then, it was focused by a lens with the focal length of 100 mm on a sample to the centre of the THz beam in the form of a spot 20-μm in diameter (at the 1/e level). The intensity of the probe radiation was 10^{10} W cm^{-2}. The induced radiation of the second harmonic

O.V. Chefonov, A.V. Ovchinnikov, M.B. Agranat Joint Institute for High Temperatures, Russian Academy of Sciences, ul. Izhorskaya 13 stroenie 2, 125412 Moscow, Russia;
e-mail: ovtch2006@yandex.ru

Received 30 November 2021
Kvantovaya Elektronika **52** (3) 269–273 (2022)
Translated by N.A. Raspopov

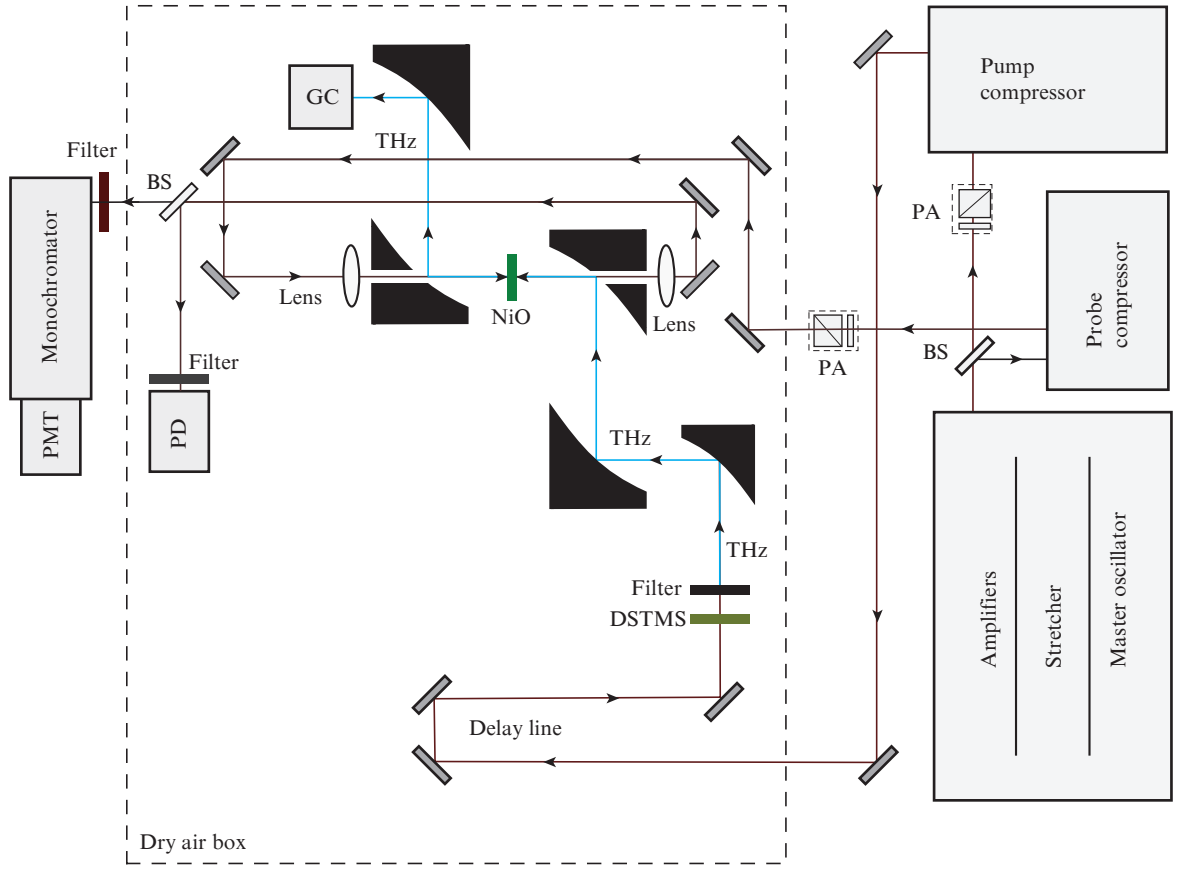

Figure 1. Experimental scheme for generation and detection of second optical harmonic in antiferromagnetic NiO under the action of terahertz radiation pulses:
(BS) light beam splitter; (PA) polarisation attenuators; (PMT) photomultiplier tube; (PD) photodiode; (GC) Golay cell.

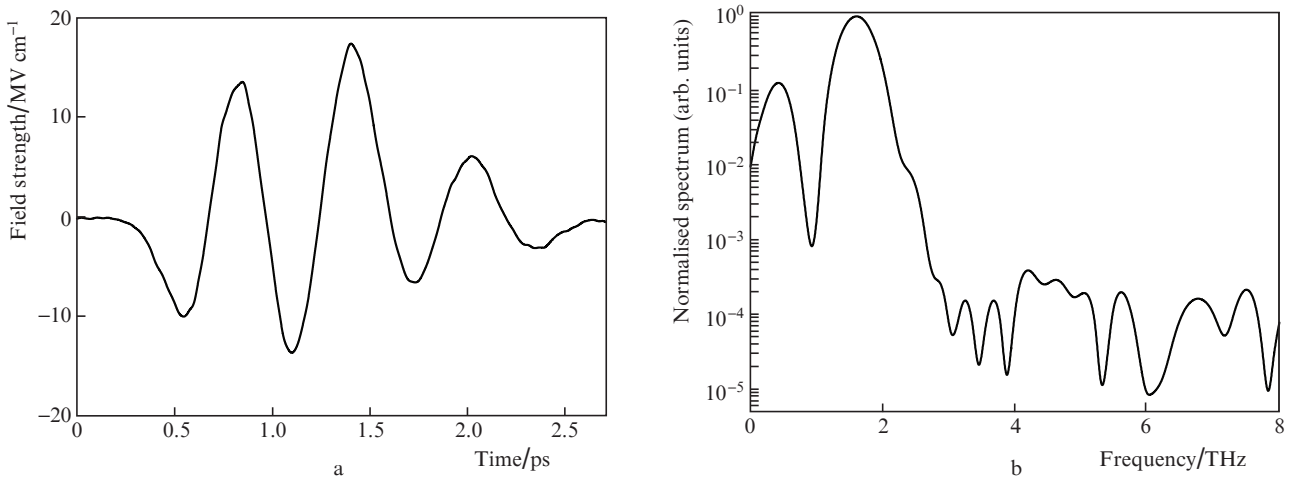

Figure 2. Time profile of (a) the electric field and (b) reconstructed Fourier-spectrum of a THz pulse.

passing from the sample was collimated by a positive lens and detected with a monochromator and a cooled photomultiplier tube. Intensities of the 1240-nm probe pulse incident on and passed through the sample were detected with an InGaAs-photodiode (DET01CFC/M, Thorlabs) with a maximum sensitivity in the range from 800 to 1700 nm. Radiation intensities of the probe pulse and second harmonic were controlled by using neutral filters.

Part of the experimental scheme responsible for generating THz pulses and studying SHG in the NiO crystal was mounted in a dry-air box at room temperature (the absolute humidity at 23 °C was 0.41 g m^{-3}). The polarisation plane of THz radiation was parallel to that of the probe pulse. In the experiments, a single-crystal NiO (111) was used with a thickness of 45 μm, a diameter of 5 mm, and both sides polished.

3. Experimental results

Transmission of the NiO crystal in the THz range is shown in Fig. 3 as a function of the maximal electric field strength of a THz pulse. The electric field strength of the latter was varied by changing the energy of the optical pulse pumping the DSTMS crystal. The transmission was determined as a ratio of the energy of THz pulse passed through NiO to that of the pulse incident onto the sample. One can see from Fig. 3 that for an electric field strength of THz pulse ranging from 0.5 to 19 MV cm^{-1}, the transmission of NiO crystal actually does not change and is, on average, 47%. Transmission of NiO in the THz spectrum range is mainly determined by the reflection losses on sample faces: $T_{\mathrm{THz}} = (1 - R_{\mathrm{THz}})^2$, where R_{THz} is the Fresnel reflection of THz radiation from an input surface of the NiO crystal.

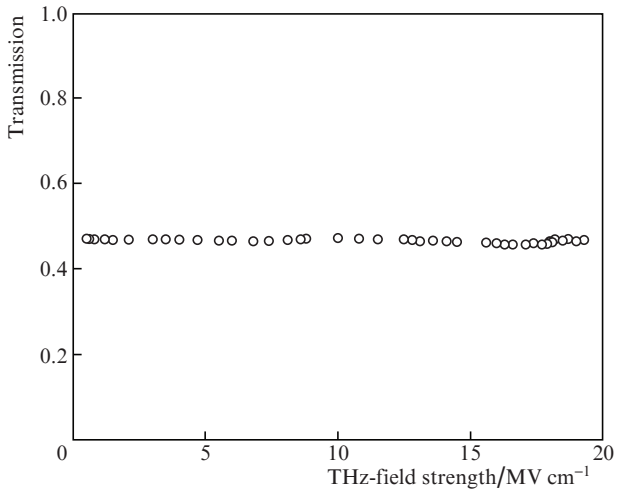

Figure 3. Transmission coefficient of the NiO crystal vs. the electric field strength of the THz pulse incident onto the sample.

Issuing from the experimental data, one can estimate the reflection and refraction coefficients of the NiO crystal for THz range: $R_{\mathrm{THz}} = 0.314$ and $n_{\mathrm{THz}} = 3.55$. These values well agree with data for certain oxides [11, 12].

Nickel oxide NiO crystallises to the cubical crystal structure (point symmetry group $m3m$) and below the Neel temperature $T_{\mathrm{N}} = 523$ K is centrosymmetric antiferromagnetic. In centrosymmetric media, even-order tensors of bulk dipole nonlinearity are zero; therefore, in an unperturbed state the electro-dipole SHG is forbidden, whereas magneto-dipole SHG is allowed and can be observed in the spectral range above 0.96 eV [13], where the absorption is related to localised transitions between 3d-sublevels of Ni^{2+} ions split in a crystal field [6]. A signal of SHG also includes a weak contribution related to quadruple effects; however, volume quadrupole effects are weak as compared to a bulk dipole contribution [14].

The electric field of a THz pulse E_Ω changes symmetry in a volume of a centrosymmetric crystal in a layer of thickness equal to about the pulse spatial size ~200 μm. In view of this fact, the symmetry vanishes, and the quadrupole susceptibility becomes distinct from zero: $\chi^{(2)} = \chi^{(2)}(E_\Omega) \neq 0$. By using the formal phenomenological approach and expanding the nonlinear susceptibility in filed series one can obtain in the first approximation the linear dependence $\chi^{(2)}(E_\Omega) = \chi^{(3)}E_\Omega$, which results in a quadratic dependence of the second harmonic intensity on the field. In this way, one can describe well known effects of the electric field-induced second harmonic (EFISH) [15, 16] and THz field-induced second harmonic (TFISH) [6, 7, 17–21]. The corresponding nonlinear polarisation has the form:

$$P(2\omega) \propto \chi^{(3)}E_\Omega E_\omega E_\omega, \tag{1}$$

where $\chi^{(3)}$ is the phenomenological tensor of bulk dipole cubic susceptibility of a medium, which does not vanishe in centrosymmetric media; and E_ω is the electric field of IR laser radiation. In addition, the symmetry may be broken at the interface in a thin near-surface layer with a thickness of several interatomic distances, which also possesses a second-order nonlinear susceptibility and may contribute into SHG [22–24]. However, as opposed to the previous work [6], we observed no SHG signal in experiments with an absent THz field, or this signal was beyond the detector sensitivity limit.

Dependences of the SH intensity on the delay time Δt between the THz pump pulse and optical probe pulse are presented in Fig. 4 for various values of the maximum electric field strength. The SH radiation was linearly polarised, and the polarisation plane coincided with that of the probe pulse radiation. One can see from Fig. 4 that with a growing electric field strength of the THz pulse, the SH intensity proportionally increases, the time profile of the latter not changing substantially. In the delay range 0–1 ps, the time profile of the SH intensity should correspond to the squared field time profile of the THz pulse (see Fig. 2a); however, it was not observed in the experiment. Probably, the transformation of the time profile for the SH intensity is related to propagation effects for THz and optical pulses in a NiO crystal.

This can be explained as follows. In the experiment, transmission of a 45-μm-thick NiO crystal at a probe pulse wavelength of 1240 nm T_ω is 4.7%. Data on optical constants for NiO [25–27] and the value of T_ω yield the estimate for the radiation absorption at the fundamental frequency and SH frequency: $\alpha_\omega \approx 600$ cm^{-1} and $\alpha_{2\omega} \approx 400$ cm^{-1}. Hence, the

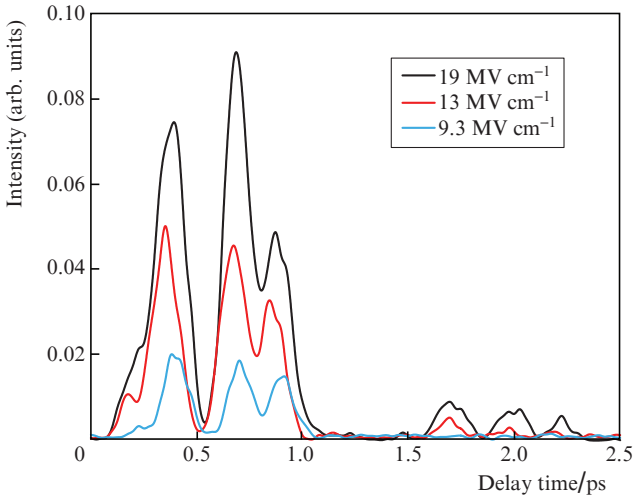

Figure 4. (Colour online) Temporal profiles of the second harmonic intensity at various values of the electric field strength of a THz pulse.

penetration depth for the SH radiation with a wavelength of 620 nm in bulk NiO will be $l_p = 1/\alpha_{2\omega} \approx 25$ μm. In this case, the coherence length $l_c = \lambda/(4\Delta n)$ [28] is the characteristic dimension of the domain, within which the maximum repumping of the fundamental-frequency radiation to the second harmonic and vice versa occurs. This coherence length is about 3–6 μm for the NiO sample refraction coefficient at the fundamental frequency $n_\omega = 2.32 \pm 0.01$ and at the second harmonic frequency we have $n_{2\omega} = 2.39 \pm 0.01$ ($\Delta n = n_{2\omega} - n_\omega$). Hence, in experiments we will detect radiation with a wavelength of 620 nm at the NiO crystal output, emitted from the depth of at most 25 μm, which corresponds to the THz pulse duration $\Delta\tau \approx 300$ fs in the sample. Thus, the SHG profile will be distorted due to a discrete character of the THz-pulse time profile with a time step of $\Delta\tau$.

After the termination of the THz pulse, a series of peaks in the second harmonic intensity is observed with time delays ranging from 1.5 to 2.5 ps (see Fig. 4). Estimates show that the delays correspond to twice the refraction time for THz pulses in the NiO sample of thickness 45 μm with the refraction coefficient $n = 3.55$.

As used here, the dependences of instantaneous intensities of SH and THz fields cannot be analysed; it seems more reasonable to consider the dependence of an integral output of SH radiation on the maximum electric field strength of a THz pulse. Figure 5 presents the dependence of output SH radiation from the NiO sample obtained from time-integrated profiles of its intensity in the interval from 0 to 1.2 ps (see Fig. 4) on the maximal electric field intensity of the THz pulse. One can see from Fig. 5 that in the range of field strengths from 6 to 19 MV cm^{-1}, the SH output is approximated by a power function with the exponent 2, which confirms the electro-dipole character of SHG.

Since in the spectrum of the THz pulse (see Fig. 2b) the component at a frequency of 1THz corresponding to the antiferromagnetic resonance in NiO is strongly suppressed due to photon absorption in a DSTMS crystal, no coherent spin precession can be resonantly induced in NiO by a magnetic field of the THz pulse. Hence, the contribution to SHG related to the action of the magnetic field of the THz pulse is either absent, or very weak. Otherwise, the time dependence of SHG should oscillate with an antiferromagnetic resonance frequency of 1 THz.

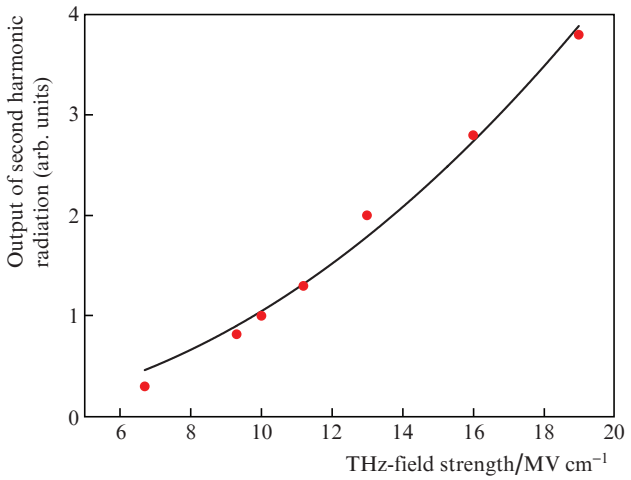

Figure 5. (Colour online) Integral dependence of second harmonic radiation at the NiO sample output on the electric field strength of a THz pulse: points correspond to experiment and the curve is the approximation by the equation $y = ax^b$ with $a = 0.00943 \pm 0.00296$ and $b = 2.04485 \pm 0.11248$.

4. Conclusions

Second harmonic generation was experimentally studied in centrosymmetric antiferromagnetic NiO under the action of THz radiation pulses with the electric field strength of up to 20 MV cm^{-1} according to the pump–probe scheme. In this scheme, the THz pulse propagates towards the optical pulse. Transmission of the NiO crystal was measured in the optical and THz spectral ranges. An analysis of the experimental data shows that the action of the electric component of THz pulse results in a dynamic loss of the centre of inversion in antiferromagnetic NiO, which is centrosymmetric from the viewpoint of crystallographic and magnetic symmetries. This effect is accompanied by removal of prohibition on generation of the electro-dipole second optical harmonic. The results obtained illustrate the importance of taking into account propagation effects for THz pulses while interpreting results of nonlinear-optical time-resolved experiments.

Acknowledgements. Experiments were performed on a unique terawatt Cr:forsterite laser system (UNU "LTFK") at a Laser femtosecond complex shared facilities centre of the Joint Institute for High Temperatures, Russian Academy of Sciences. The work was supported by the Russian Foundation for Basic Research (Project No. 20-08-00627).

References

1. Mishina E.D., Sherstyuk N.E., Barskiy D.R., Sigov A.S., Golovko Y.I., Mukhorotov V.M., De Santo M., Rasing T. *J. Appl. Phys*., **93** (10), 6216 (2003).
2. Yokota H., Kaneshiro J., Uesu Y. *Phys. Res. Int*., **2012**, 704634 (2012).
3. Fiebig M., Pavlov V.V., Pisarev R.V. *J. Opt. Soc. Am. B*, **22** (1), 96 (2005).
4. Meshulam G., Berkovic G., Kotler Z., Sa'ar A. *Rev. Sci. Instrum*., **71** (9), 3490 (2000).
5. Cornet M., Degert J., Abraham E., Freysz E. *Opt. Lett*., **39** (20), 5921 (2014).
6. Ovchinnikov A.V., Chefonov O.V., Agranat M.B., Grishunin K.A., Il'in N.A., Pisarev R.V., Kimel' A.V., Kalashnikova A.M. *JETP Lett*., **104** (7), 441 (2016) [*Pis'ma Zh. Eksp. Teor. Fiz*., **104** (7), 467 (2016)].
7. Grishunin K.A., Ilyin N.A., Sherstyuk N.E., Mishina E.D., Kimel A., Mukhortov V.M., Ovchinnikov A.V., Chefonov O.V., Agranat M.B. *Sci. Rep*., **7** (1), 687 (2017).
8. Kirilyuk A., Rasing T. *J. Opt. Soc. Am. B*, **22** (1), 148 (2005).
9. Agranat M.B., Ashitkov S.I., Ivanov A.A., Konyashchenko A.V., Ovchinnikov A.V., Fortov V.E. *Quantum Electron*., **34** (6), 506 (2004) [*Kvantovaya Elektron*., **34** (6), 506 (2004)].
10. Chefonov O.V., Ovchinnikov A.V., Evlashin S.A., Agranat M.B. *J. Infrared Millim. Terahertz Waves*, **39** (11), 1047 (2018).
11. Jin Z., Mics Z., Ma G., Cheng Z., Bonn M., Turchinovich D. *Phys. Rev. B*, **87**, 094422 (2013).
12. Zibold A., Liu H.L., Moore S.W., Graybeal J.M., Tanner D.B. *Phys. Rev. B*, **53**, 11734 (1996).
13. Fiebig M., Fröhlich D., Lottermoser T., Pavlov V.V., Pisarev R.V. Weber H.-J. *Phys. Rev. Lett*., **87**, 137202 (2001).
14. Cazzanelli M., Schilling J. *Appl. Phys. Rev*., **3** (1), 011104 (2016).
15. Aktsipetrov O.A., Fedyanin A.A., Mishina E.D., Rubtsov A.N., van Hasselt C.W., Devillers M.C., Rasing T. *Phys. Rev. B*, **54** (3), 1825 (1996).
16. Meshulam G., Berkovic G., Kotler Z., Sa'ar A. *Rev. Sci. Instrum*., **71** (9), 3490 (2000).

17. Nahata A., Heinz T.F. *Opt. Lett*., **23** (1), 67 (1998).
18. Chen J., Han P., Zhang X.-C. *Appl. Phys. Lett*., **95** (1), 011118 (2009).
19. Cook D., Chen J., Morlino E., Hochstrasser R. *Chem. Phys. Lett*., **309** (3), 221 (1999).
20. Cornet M., Degert J., Abraham E., Freysz E. *Opt. Lett*., **39** (20), 5921 (2014).
21. Ovchinnikov A.V., Chefonov O.V., Mishina E.D., Agranat M.B. *Sci. Rep*., **9** (1), 9753 (2019).
22. Aktsipetrov O.A., Bessonov V.O., Fedyanin A.A., Valdner V.O. *JETP Lett*., **89** (2), 58 (2009) [*Pis'ma Zh. Eksp. Teor. Fiz*., **89** (2), 64 (2009)].
23. Tom H.W.K., Heinz T.F., Shen Y.R. *Phys. Rev. Lett*., **51**, 1983 (1983).
24. Epperlein D., Dick B., Marowsky G., Reider G.A. *Appl. Phys. B*, **44**, 5 (1987).
25. Rao K.V., Smakula A. *J. Appl. Phys*., **36** (6), 2031 (1965).
26. Powell R.J., Spicer W.E. *Phys. Rev. B*, **2**, 2182 (1970).
27. Huber L., Ferrer A., Kubacka T., Huber T., Dornes C., Sato T., Ogawa K., Tono K., Katayama T., Inubushi Y., Yabashi M., Tanaka Y., Beaud P., Fiebig M., Scagnoli V., Staub U., Johnson S.L. *Phys. Rev. B*, **92**, 094304 (2015).
28. Akhmanov S.A., Kovrigin A.I., Khokhlov R.V., Chunaev O.N. *J. Exp. Theor. Phys*., **18**, 919 (1964) [*Zh. Eksp. Teor. Fiz*., **45** (4), 1336 (1964)].